Journal of Metals, Materials and Minerals, 34(1), 1833, 2024

First-principles study on structural and electronic properties of P3HT-graphene

Fia AMALIA[1], Ari Dwi NUGRAHENI[1], and Sholihun SHOLIHUN[1,*]

[1] *Department of Physics, Faculty of Mathematics and Natural Sciences, Universitas Gadjah Mada, Sekip Utara BLS 21, Yogyakarta 55281, Indonesia*

***Corresponding author e-mail**: sholihun@ugm.ac.id

Received date:
3 September 2023
Revised date
15 December 2023
Accepted date:
11 March 2024

Keywords:
P3HT-Graphene;
Adsorption energy;
Electron transfer

Abstract

Based on density functional theory, calculations have been carried out to study the structural and electronic properties of the polymer Poly (3-hexylthiophene) (P3HT) interacting with monolayer graphene as an active layer. $(P3HT)_1$-graphene and $(P3HT)_2$-graphene are optimized on graphene using the generalized-gradient-approximation type of the exchange-correlation functional. Adsorption energy, band gap, and charge transfer are calculated. The calculated adsorption energy shows that all systems have negative adsorption energy, indicating that the reaction is exothermic. Compared to $(P3HT)_1$-graphene, $(P3HT)_2$-graphene has a lower band gap. As for the charge transfer calculation, a negative ΔN indicates that electron transfers from P3HT to graphene.

1. Introduction

In recent years, many efforts have been devoted to investigating organic photovoltaic (OPV) devices based on bulk heterojunctions of fullerenes as an acceptor and poly(3-hexylthiophene) (P3HT) as a donor [1-8]. Fullerene derivatives are interpreted as acceptors due to their unique characteristics. The photovoltaic cells based on such derivatives have very high electron transport and isotropic charge mobility [9]. However, fullerene derivatives have several disadvantages, including donor and acceptor differences in energy levels, not only in high energy losses but also in open circuit voltage drop (V_{OC}). Bulk heterojunction organic solar cells based on P3HT and PCBM generate specific physical constraints, including limited absorption in the visible region and high manufacturing costs [10]. More recently, graphene photovoltaic cells have been used as electron acceptors (energy level alignment) instead of the fullerene derivative. Graphene is particularly promising for OPV owing to its high charge mobility and two-dimensional structure. Graphene is a carbon nanomaterial containing a monolayer of sp2 carbon atoms settled in a two-dimensional honeycomb structure. It has a very high electron mobility of 2.5×10^5 $cm^2 \cdot V^{-1} \cdot s^{-1}$ and high electrical conductivity (10^8 $S \cdot m^{-2}$), high transparency (absorbance of 2.3%), and large specific surface area (2.63×10^6 $m^2 \cdot kg^{-1}$). This material was also demonstrated to be stable at ambient conditions [11]. It displays exceptional room temperature thermal conductivity, in the order of 5000 $Wm^{-1} \cdot K^{-1}$ higher than that of copper or any other known material. Graphene can act as both a metal and a semiconductor. It can conduct electricity better than copper and simultaneously has conduction and valence bands as in semiconductors but with no band gap; therefore, it is known as a semimetal [12,13].

To improve the OPV efficiency, careful consideration must be given to band gap, energy level, and compatibility of materials used with balanced, open circuit voltage (V_{OC}), short circuit current density (I_{SC}), and charge factor (FF), which are limited by the properties of their intrinsic materials (donor and acceptor) [14-16]. To balance the I_{SC}, V_{OC}, and FF parameters to be maximized simultaneously, a low band gap of the conjugated polymer is required; the band gap energy must be below 2 eV. A slight energy difference between the LUMO at the donor and the LUMO at the acceptor is needed to achieve optimal charge transfer. The wide band gap of P3HT is an obstacle to increasing OPV efficiency [17]. Therefore, it is necessary to synergize between graphene-based acceptor materials and donor polymers in photoactive layers to generate increased photon yield, enhanced exciton, effective exciton dissociation, and efficient charge transport [18]. This study chose graphene as an acceptor material because it has a band gap energy of around zero, excellent optical, electrical, chemical, mechanical, and thermal properties, and a large surface area and flexibility [19].

Research on P3HT donor materials has been carried out experimentally and computationally. P3HT experimental research has been chosen as a donor material for organic solar cells, and fullerene has been selected as an acceptor material [1-8]. Kim *et al*. demonstrated the surface-mediated self-assembly of P3HT on a graphene monolayer; their study has been carried out experimentally and computationally. The face-on configuration of P3HT on graphene was favorable because of the $\pi - \pi$ interactions between the thiophene backbone of P3HT and graphene. These findings also indicate that alkyl chains and thiophene backbones in P3HT are essential to determine the molecular configuration of P3HT on the graphene surface [20].

Noori *et al*., based on large atomistic models of the graphene/polymer interface, indicate that the ideal open-circuit voltage approaches one volt and that epoxide functional groups can dramatically affect the photovoltage. Their findings suggest that the selective removal of epoxide groups and using ultra disperse polymers are crucial to achieving graphene solar cells with improved energy conversion efficiency [21]. DFT-based theoretical calculations are carried out to design the optimal molecular geometry to get the proper adsorption process, interactions between molecules, and electronic properties to increase organic solar cells' efficiency. In this study, P3HT and graphene were modeled as active materials for organic solar cells.

2. Methods

Density functional theory (DFT) based calculations have been performed using the PHASE [22-25] package to explain the structural geometries and electronic properties. The generalized gradient approximation (GGA) function, according to the Perdew-Burke-Ernzerhof (PBE) parameterization, was applied for exchange and correlation energies [26]. Brillouin zone integration was approximated using a 4-point mesh grid. The plane-wave kinetic energy cutoff of the electron wave functions and charge density were set to 25Ry and 225Ry, respectively. Graphene calculations were performed with an 8 × 8 × 8 supercell with a 16.0 Å vacuum. The atomic relaxation was achieved until the forces on each atom were less than (5.0×10^{-3} eV·Å^{-1}).

The first step to modeling the P3HT-graphene system is to optimize the lattice parameter of graphene. An optimum lattice constant is determined by fitting the calculated total energies versus varied lattice parameters (Figure 1) using the Birch-Murnaghan Equation of State (BM-EOS). The BM-EOS is given as follows:

$$E(V) = E_0 + \frac{9}{16}V_0B_0\left[\left((W)^{\frac{2}{3}}-1\right)^3 B_0' + \left((W)^{\frac{2}{3}}-1\right)^2\left(6-4(W)^{\frac{2}{3}}\right)\right] \quad (1)$$

where $W=\frac{V_0}{V}$. The fitting parameters E_0, V_0, B_0, and B_0' are the optimized total energy, lattice volume, bulk modulus, and the first derivative of B_0 at the constant volume, respectively [27,28].

Once an optimized lattice constant is obtained, graphene is enlarged to be a supercell consisting of 128 carbon atoms. Next, P3HT is modeled from a long chain of polymer and thiophenes in which sulfur is connected in a heterocycle position [29]. The P3HT construction is carried out in the phase viewer by inputting thiophene coordinates, which are then added to polymer chains (Figure 2). P3HT systems are variably constructed with two P3HT monomers. $(P3HT)_2$ is modeled by connecting the side heads of both P3HT units.

In this work, the distance between the graphene and P3HT was initially set so that P3HT is parallel with the graphene surface (Figure 3). Furthermore, atoms were relaxed to find the optimized geometry of the graphene-P3HT system.

The adsorption properties and relaxation behavior are then analyzed using adsorption energy (E_{ads}). A negative E_{ads} value indicates that the process reveals an exothermic reaction [30]. The adsorption energy E_{ads} is expressed as follows [31,32]:

$$E_{ads} = E_{Graphene+P3HT} - \left(E_{Graphene} + E_{P3HT}\right) \quad (2)$$

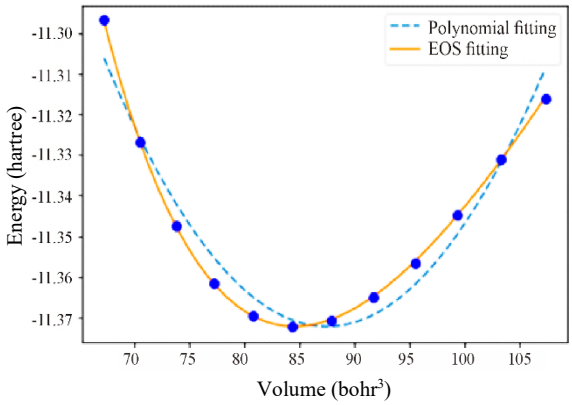

Figure 1. The BM-EOS fitting result of energy and volume.

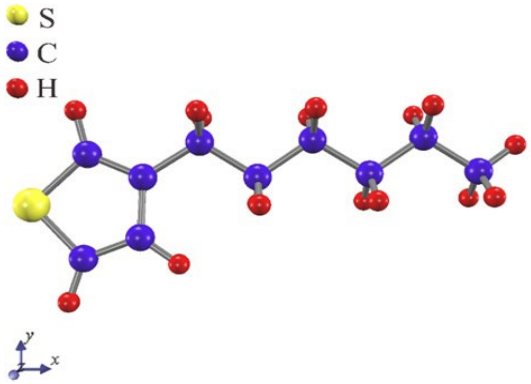

Figure 2. The P3HT structure. Blue, red, and yellow balls are carbon, hydrogen, and sulfur, respectively.

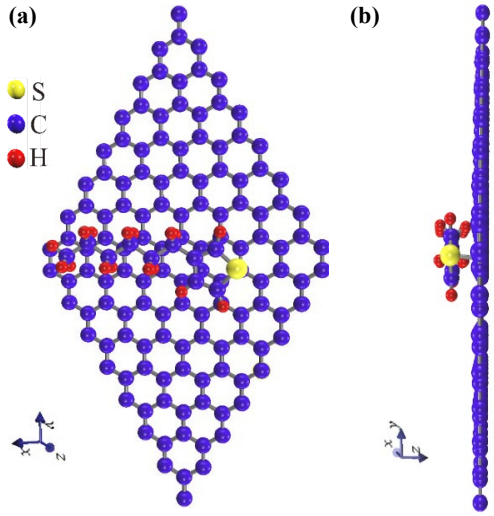

Figure 3. (a) (P3HT)1-graphene structure (top views), and (b) (P3HT)1-graphene structure (side views).

3. Results and discussion

The lattice parameters are varied, and their energies are calculated to obtain an optimized lattice constant. Applying the BM-EOS (Equation (1)), graphene's calculated optimized lattice constant is 2.48Å. This value is in agreement with the experimental data of 2.48Å [33].

As shown in Figure 4(a), P3HT is a single unit consisting of 27 atoms in which 16 atoms of hydrogen, 10 atoms of carbon, and 1 atom of Sulphur are bonded, while $(P3HT)_2$ consists of 52 atoms in which 30 atoms of hydrogen, 20 atoms of carbon, and 2 atoms of Sulphur are bonded (Figure 4(b)).

The bond lengths and bond angles between atoms for P3HT, $(P3HT)_2$, $(P3HT)_1$-graphene, and $(P3HT)_2$-graphene are given in Tables 1 and Table 2, respectively. The calculated results are close to those of the previous study [17]. The deviations of bond length between our result and that in Ref. [17] are tiny, i.e., 0.01 Å to 0.03 Å for P3HT and 0.01 Å to 0.04 Å for $(P3HT)_2$. In Ref. [17], the bond length and angle calculated for the 6-mer are close to experimental values. The deviations for the bond lengths are less than 0.002, and those for the bond angles are less than 2°**.** In our calculations, the deviations of bond angles are 0.25° to 1.56° for P3HT and 0.04° to 3.04° for $(P3HT)_2$. As for $(P3HT)_1$-graphene and $(P3HT)_2$-graphene, there is no reference to compare.

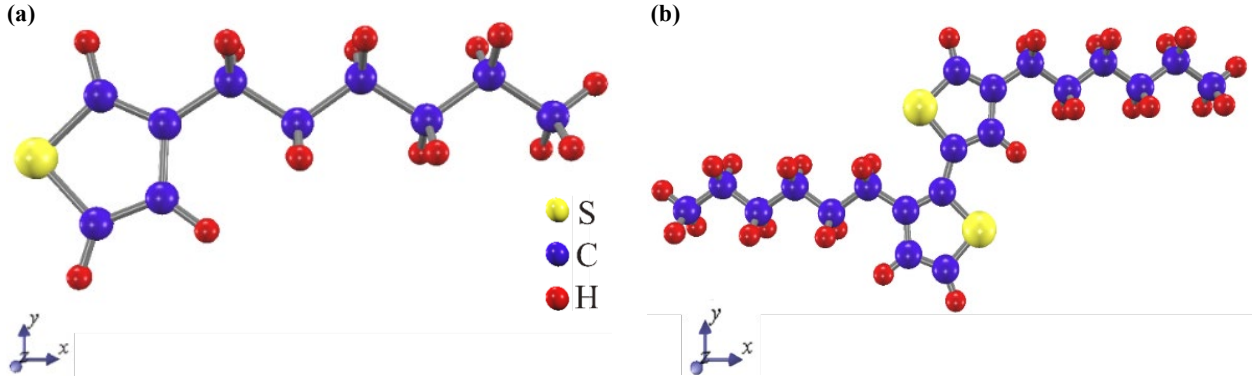

Figure 4. Geometry optimizations of (a) $(P3HT)_1$, and (b) $(P3HT)_2$.

Table 1. The calculated bond lengths and DFT research reference.

System	Bond lengths	Present work (Å)	Reference [17] (Å)	Δ (Å)
P3HT	S(1)-C(5)	1.75	1.74	0.01
	S(1)-C(4)	1.75	1.76	0.01
	C(5)-C(3)	1.38	1.37	0.02
	C(3)-C(2)	1.45	1.42	0.03
	C(2)-C(4)	1.38	1.38	0.00
$(P3HT)_2$	S(1)-C(5)	1.75	1.74	0.01
	S(1)-C(4)	1.77	1.76	0.01
	S(27)-C(31)	1.78	1.76	0.02
	S(27)-C(30)	1.75	1.76	0.01
	C(3)-C(5)	1.39	1.37	0.02
	C(2)-C(3)	1.44	1.42	0.02
	C(4)-C(2)	1.40	1.38	0.02
	C(31)-C(4)	1.47	1.45	0.02
	C(31)-C(29)	1.40	1.38	0.02
	C(29)-C(28)	1.44	1.41	0.03
	C(28)-C(30)	1.38	1.38	0.00
$(P3HT)_1$-G	S(129)-C(132)	1.73	-	-
	S(129)-C(133)	1.73	-	-
	C(131)-C(133)	1.38	-	-
	C(130)-C(131)	1.44	-	-
	C(132)-C(130)	1.38	-	-
$(P3HT)_2$-G	S(1)-C(5)	1.73	-	-
	S(1)-C(4)	1.75	-	-
	S(27)-C(31)	1.75	-	-
	S(27)-C(30)	1.72	-	-
	C(3)-C(5)	1.38	-	-
	C(2)-C(3)	1.43	-	-
	C(4)-C(2)	1.39	-	-
	C(31)-C(4)	1.46	-	-
	C(31)-C(29)	1.40	-	-
	C(29)-C(28)	1.43	-	-
	C(28)-C(30)	1.38	-	-

Table 2. The calculated bond angles and DFT research reference.

System	Bond angle (°)	Present work (°)	Reference [17] (°)	Δ (°)
P3HT	C(5)-S(1)-C(4)	91.32	91.78	0.46
	S(1)-C(5)-C(3)	112.40	111.66	0.74
	C(5)-C(3)-C(2)	111.35	112.92	1.56
	C(3)-C(2)-C(4)	113.39	113.64	0.25
	C(2)-C(4)-S(1)	111.54	110.01	1.53
	S(1)-C(4)-H(7)	119.68	120.90	1.23
	H(2)-C(4)-C(7)	128.79	129.09	0.31
$(P3HT)_2$	C(5)-S(1)-C(4)	91.81	91.78	0.04
	C(30)-S(27)-C(31)	91.78	92.15	0.37
	C(3)-C(5)-S(1)	112.43	111.66	0.77
	C(2)-C(3)-C(5)	111.64	112.92	1.28
	C(4)-C(2)-C(3)	114.61	113.64	0.97
	S(1)-C(4)-C(2)	109.51	110.01	0.50
	C(31)-C(4)-S(1)	122.72	120.90	1.82
	C(31)-C(4)-C(2)	127.77	129.09	1.32
	S(27)-C(31)-C(4)	117.76	120.80	3.04
	S(27)-C(31)-C(29)	110.63	110.07	0.56
	C(29)-C(31)-C(4)	117.76	129.13	2.48
	C(31)-C(29)-C(28)	112.00	113.92	1.91
	C(29)-C(28)-C(30)	113.96	113.87	0.10
	C(28)-C(30)-S(27)	111.62	110.00	1.62
	S(27)-C(30)-H(33)	119.42	120.85	1.43
	H(33)-C(30)-C(28)	128.96	129.15	0.19
$(P3HT)_1$-G	C(132)-S(129)-C(133)	91.90	-	-
	S(129)-C(133)-C(131)	112.34	-	-
	C(133)-C(131)-C(130)	111.13	-	-
	C(131)-C(130)-C(132)	113.26	-	-
	C(130)-C(132)-S(129)	111.37	-	-
	S(129)-C(132)-H(135)	120.04	-	-
	H(135)-C(132)-C(130)	128.59	-	-
$(P3HT)_2$-G	C(5)-S(1)-C(4)	92.43	-	-
	C(30)-S(27)-C(31)	92.50	-	-
	C(3)-C(5)-S(1)	112.40	-	-
	C(2)-C(3)-C(5)	111.26	-	-
	C(4)-C(2)-C(3)	114.45	-	-
	S(1)-C(4)-C(2)	109.45	-	-
	C(31)-C(4)-S(1)	123.08	-	-
	C(31)-C(4)-C(2)	127.42	-	-
	S(27)-C(31)-C(4)	117.67	-	-
	S(27)-C(31)-C(29)	110.72		
	C(29)-C(31)-C(4)	131.60		
	C(31)-C(29)-C(28)	111.57		
	C(29)-C(28)-C(30)	113.85		
	C(28)-C(30)-S(27)	111.35		
	S(27)-C(30)-H(33)	120.08		
	H(33)-C(30)-C(28)	128.57		

The atomic configuration of the $(P3HT)_n$ and $(P3HT)_n$-graphene systems (n = 1, 2) are shown in Figure 5 and Figure 6. In the $(P3HT)_1$-graphene, P3HT is floating 5.5 Å above graphene and makes no bond with graphene. Thus, P3HT interacts with graphene through a weak interaction. The carbon bonds in hexyl are sp^3 orbitals, while those in graphene have sp^2 orbitals. During optimization of $(P3HT)_2$-graphene, a hydrogen atom is released from P3HT to graphene, leaving a carbon atom of P3HT with three bonds. Forming a stable sp^3 configuration, this carbon is bonded by carbon from graphene. The hydrogen released from P3HT is then connected by a carbon from graphene, forming a sp^3 configuration.

We next plot the density of states (DOS) for each system in Figure 7. The calculated DOS is then smoothed using Gaussian fitting. The peak on the left side of the DOS represents the HOMO energy level, the right represents LUMO, and the unoccupied region indicates the band gap between the HOMO and LUMO energies [34]. Graphene is a semimetal material with zero band gap (Figure 7(a) and Figure 7(f)), while P3HT behaves as a semiconductor (Figure 7(b)) with a calculated band gap energy of 2.95 eV (Table 3). The band gap decreases significantly to 1.87 eV (Figure 7(c)) when P3HT is duplicated as $(P3HT)_2$ in Figure 4(b). When $(P3HT)_1$ is introduced to graphene (Figure 7(d)), a small gap of 50 meV is open.

Table 3. The calculated HOMO, LUMO, and gap energy of each system.

System	E_{LUMO} (eV)	E_{HOMO} (eV)	E_{Gap} (eV)
$(P3HT)_1$	5.06	2.12	2.95
$(P3HT)_2$	3.31	1.44	1.87
$(P3HT)_1$-G	0.32	0.27	0.05
$(P3HT)_2$-G	0.14	0.10	0.04

Meanwhile, when $(P3HT)_2$ interacts with graphene (Figure 7(e)), the band gap decreases to 40 meV. The calculated band gap of P3HT agrees with that in Ref. [17] that the band gap decreases with an increasing number of chain bonds in P3HT. Lubis and Mineo [17] calculated the band gaps of these polymers by fitting the finite size of oligomers. The band gap calculations of finite-size oligomers were conducted using hybrid density functional theory with B3LYP/6-31G (d,p). The HOMO-LUMO energy gaps were fitted, and the band gap of infinite-length polymers was estimated. Using an extrapolation scheme from DFT results, Lubis and Mineo obtained the band gap of P3HT of 1.81 eV, which is very close to our result (1.87 eV).

We calculate the adsorption energy (Eads) using Equation (2) to examine the interaction between molecules and graphene. A negative E_{ads} value indicates that the process is an exothermic reaction [30]. A negative value of E_{ads} suggests that a molecule is adsorbed by graphene, while a positive value indicates that no adsorption occurs. The calculated results given in Table 4 show that $(P3HT)_1$ and $(P3HT)_2$ are adsorbed by graphene, and the systems experience an exothermic reaction. To determine the distance between the P3HT and graphene molecule, the distance Rz S is the distance of the sulfur atom in P3HT along the z-axis, and Rz C is the distance of the C atom in graphene along the z-axis. It can be seen in Table 5 that the molecular distance in $(P3HT)_2$-graphene is larger than $(P3HT)_1$-graphene. This follows the value of E_{ads} of the $(P3HT)_1$-graphene, which is more negative, or the P3HT molecules are more adsorbed by graphene because the molecular distance is closer between P3HT and graphene.

We carry out charge transfer (Q) calculations following the work in Ref. [35] that charge transfer is defined as $Q=\frac{(\mu_A-\mu_B)}{2(\eta_A+\eta_B)}$, where μ and η are chemical potential and hardness, respectively. The charge transfers from A to B if Q is negative, and vice versa. Our calculated result in Table 5 shows that both systems have a negative value of Q, indicating that charge flows from P3HT to graphene. Thus, P3HT behaves as an electron donor, and graphene acts as an acceptor.

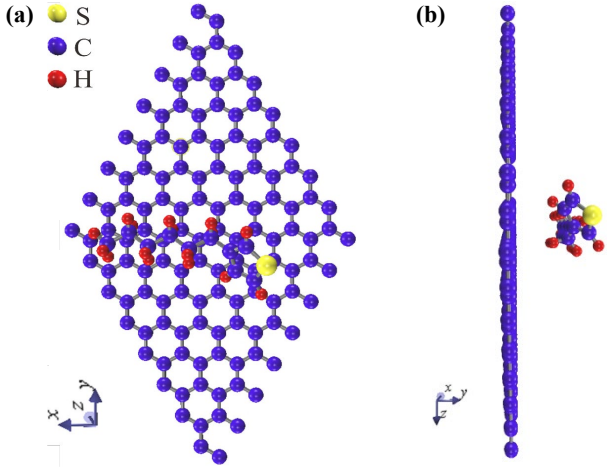

Figure 5. Optimized geometry of (a) $(P3HT)_1$-graphene (top views) and (b) $(P3HT)_1$-graphene (side views).

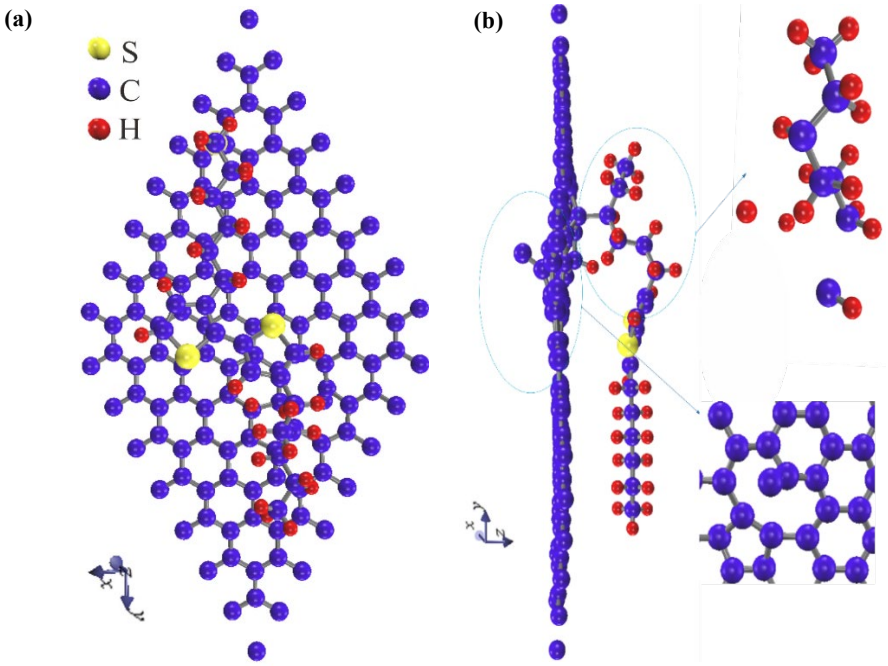

Figure 6. Optimized geometry of $(P3HT)_2$-graphene (top views) and $(P3HT)_2$-graphene (side views).

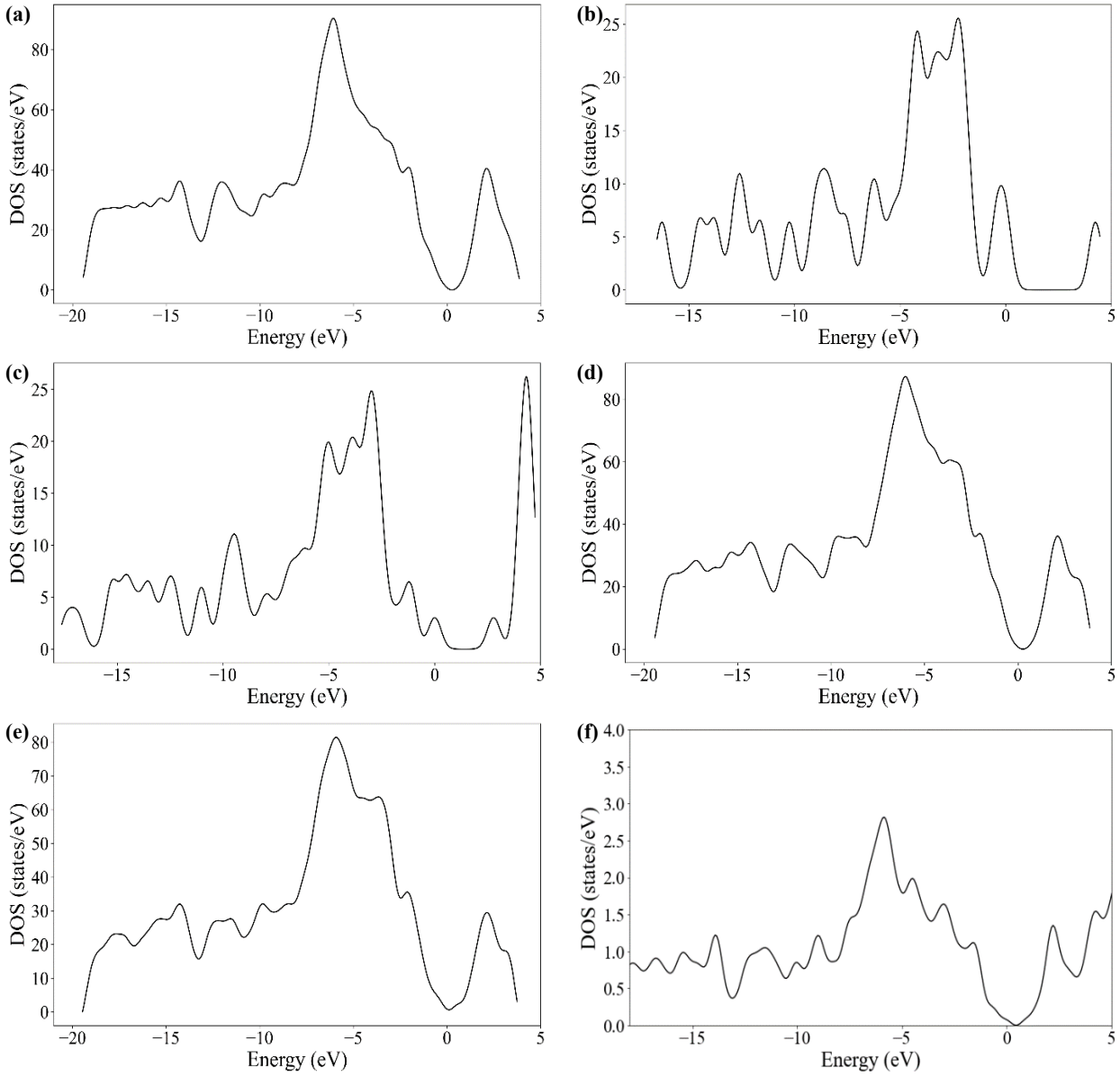

Figure 7. DOS plots of (a) pristine graphene supecell, (b) $(P3HT)_1$, (c) $(P3HT)_2$, (d) $(P3HT)_1$-graphene, (e) $(P3HT)_2$-graphene, and (f) pristine graphene unit cell.

Table 4. Calculated adsorption energy for $(P3HT)_1$-graphene and $(P3HT)_2$-graphene systems.

System	E_{ads} (eV)	Rz S (Å)	Rz C (Å)
$(P3HT)_1$-graphene	-13.44	2.81	8.31
$(P3HT)_2$-graphene	-12.43	21.44	13.53

Table 5. Charge transfer of $(P3HT)_1$-graphene and $(P3HT)_2$-graphene systems.

System	E_{LUMO} (eV)	E_{HOMO} (eV)	E_{Gap} (eV)	μ (eV)	η (eV)	Q (e)
$(P3HT)_1$	4.15	0.10	4.05	2.13	2.03	-
$(P3HT)_2$	2.70	0.09	2.61	1.39	1.31	-
$(P3HT)_1$-graphene	0.49	0.09	0.41	0.29	0.20	-0.41
$(P3HT)_2$-graphene	0.34	0.07	0.27	0.21	0.14	-0.37

4. Conclusion

Two systems of $(P3HT)_1$-graphene and $(P3HT)_2$-graphene were optimized, and it was found that both systems have negative adsorption energy, indicating that the reaction is exothermic. Adding P3HT decreases the band gap either in the $(P3HT)_n$ system or in the $(P3HT)_n$-graphene system. From the calculated charge transfer, electrons flow from P3HT to graphene, indicating that P3HT acts as an electron donor and as an acceptor.

Acknowledgements

The DFT calculations were carried out using the ALELEON Supercomputer at EFISON Lisan Teknologi HQ, Indonesia.

References

[1] D. Sukeguchi, S. P. Singh, M. R. Reddy, H. Yoshiyama, R. A. Afre, Y. Hayashi, H. Inukai, T. Soga, S. Nakamur, N. Shibata, and T. Toru, "New diarylmethano fullerene derivatives and their properties for organic thin-film solar cells," *Beilstein Journal of Organic Chemistry*, vol. 5, no. 7, pp. 1-10, 2009.

[2] Y. Wang, J. Chen, H. D. Kim, B. Wang, R. Iriguchi, and H. Ohkita, "Ternary blend solar cells based on a conjugated polymer with diketopyrrolopyrrole and carbazole units," *Frontiers in Energy Research*, vol. 6, no. 113, 2018.

[3] M. S. Ulum, E. Sesa, Kasman, and W. Belcher, "The effect of active layer thickness on P3HT:PCBM nanoparticulate organic photovoltaic device performance," *Journal of Physics: Conference Series*, vol. 1242, p. 012025, 2019.

[4] C. Ishan, Ghosekar, C. Ganesh, and Patil, "Impact of concentration variation and thermal annealing on performance of multilayer OSC consisting of sandwiched P3HT layer between PEDOT:PSS and P3HT:PCBM," *Microelectronic Engineering*, vol. 221, p. 111195, 2020.

[5] G. Grancharov, M. D. Atanasova, R. Kalinova, R. Gergova G. Popkirov, C. Dikov, and S. M. Vassileva, "Flexible polymer–organic solar cells based on P3HT:PCBM bulk heterojunction active layer constructed under environmental conditions," *Molecules*, vol. 26, p. 6890, 2021.

[6] T. S. T. Khanh, N. P. H. Nam, and N. N. Dinh, "Facile preparation, characterization of flexible organic solar cells using P3HT-MWCNTS composite photoactive layer," *Journal of Materials Science and Chemical Engineering*, vol. 8, pp. 1-10, 2020.

[7] P. Mahendia, G. Chauhan, H. Wadhwa, G. Kandho, S. Mahendia, R. Srivastava, O. P. Sinha, T. D. Clemons, and S. Kumar, "Study of induced structural, optical and electrochemical properties of poly (3-hexylthiophene) (P3HT), [6,6]-phenyl-C61-butyric-acid-methyl-ester (PCBM) and their blend as an effect of graphene doping," *Journal of Physics and Chemistry of Solids,* vol. 148, pp. 1-9, 2020.

[8] M. Piralaee, and A. Asgari, "Investigation of the performance parameters of P3HT: PCBM solar cell: The role of temperature," *Optik*, vol. 251, p. 168453, 2021.

[9] Y. He, and Y. Li, "Fullerene derivative acceptors for high performance polymer solar cells," *Physical Chemistry Chemical Physics,* vol. 13, pp. 1970-1983, 2011.

[10] A. Aboulouard, S. Mtougui, N. Demir, A. Moubarik, M. L. Idrissi, and M. Can, "New non-fullerene electron acceptors-based on quinoxaline derivatives for organic photovoltaic cells: DFT computational study," *Synthetic Metals*, vol. 279, p. 116846, 2021.

[11] B. Bkakri, N. Chehata, O. E. Kusmartseva, F. Kusmartsev, M. Song, and A. Bouazizi, "Charge transfer and transport properties in P3HT and P3HT:Graphene based organic solar cells," *International Journal of Scientific Research & Engineering Technology*, vol. 3, no. 2, pp. 2356-5608, 2015.

[12] X. Li, Y. Chen, S. Mo, L. Jia, and X. Shao, "Effect of surface modification on the stability and thermal conductivity of water-based SiO_2-coated graphene nanofluid," *Thermochimica Acta,* vol. 595, pp. 6-10, 2014.

[13] L. V. Davoise, A. M. D. Pascual, and R. P. Capilla, "Application of graphene-related materials in organic solar cells," *Materials*, vol. 15, pp. 1-33, 2022.

[14] J. Gao, R. Ming, Q. An, X. Ma, M. Zhang, J. Miao, J. Wang, C. Yang, and F. Zhang, "Ternary organic solar cells with J71 as donor and alloyed acceptors exhibiting 13.16% efficiency," *Nano Energy*, vol. 63, pp. 1-6, 2019.

[15] M. Abdallaoui, N. Sengouga, A. Chala, A. F. Meftah, and A. M. Meftah, "Comparative study of conventional and inverted P3HT: PCBM organic solar cell," *Optical Materials*, vol. 105, p. 109916, 2020.

[16] E. M. Mkawi, Y. A. Hadeethi, R. S. Bazuhair, A. S. Yousef, E. Shalaan, B. Arkook, A. M. A. Daiem, and A. Bekyarova, "Fabricated Cu_2Zn SnS_4 (CZTS) nanoparticles as an additive in P3HT: PCBM active layer for efficiency improvement of polymer solar cell," *Journal of Luminescence*, vol. 240, p. 118420, 2021.

[17] P. Lubis, and M. Saito, "Band gap design of thiophene polymers based on density functional theory", *Japanese Journal of Applied Physics*, vol. 53, p. 071602, 2014.

[18] E. Muchuweni, B. S. Martincigh, and V. O. Nyamori, "Organic solar cells: Current perspectives on graphene-based materials for electrodes, electron acceptors and interfacial layers," *Energy research,* vol. 45, no. 5, pp. 6518-6549, 2020.

[19] A. K. Geim, and K. S. Novoselov, "The rise of graphene," *Nature Materials*, vol. 6, pp. 183-191, 2007.

[20] D. H. Kim, H. S. Lee, H-J. Shin, Y-S. Bae, K-H. Lee, S-W Kim, D. Choi, and J-Y. Choi, 2013, "Graphene surface induced specific self-assembly of poly(3 hexylthiophene) for nanohybrid optoelectronics: From first-principles calculation to experimental characterizations," *Soft Matter*, vol. 9, p. 5355-5360, 2013.

[21] K. Noori, D. Konios, M. M. Stylianakis, E. Kymakis, and F. Giustino, "Energy-level alignment and open-circuit voltage at graphene/ polymer interfaces: theory and experiment," *2D Materials*, vol. 3, p. 015003, 2016

[22] T. Yamasaki, A. Kuroda, T. Kato, J. Nara, J. Koga, T. Uda, K. Minami, and T. Ohno, "Multi-axis decomposition of density functional program for strong scaling up to 82,944 nodes on the k computer: Compactly folded 3d-fft communicators in the 6d torus network," *Computer Physics Communications*, vol. 244, pp. 264-276, 2019.

[23] Sholihun, W. Amalia, D. P. Hastuti, P. Nurwantoro, A. D. Nugraheni, and R. H. S. Budhi, "Magic vacancy-numbers in h-BN multivacancies: The first-principles study," *Materials Today Communications,* vol. 20, p. 100591, 2019.

[24] Z. S. Fatomi, A. D. Nugraheni, and Sholihun, "Vibrational effect on vacancy concentration in diamond: The density-functional-theory calculation," *Computational Condensed Matter,* vol. 32, p. e00708, 2022.

[25] F. Amalia, "Study on electronic structure of donor-acceptor materials based on P3HT-graphene employing density functional theory," *Thesis,* Universitas Gadjah Mada, 2023.

[26] S. A. Roncancio, A. A. G. Blanco, D. H. Linares, and K. Sapag, "DFT study of hydrogen adsorption on Ni/graphene," *Applied Surface Science*, vol. 447, pp. 254-260, 2018.

[27] D. P. Hastuti, P. Nurwantoro, and Sholihun, "Stability study of germanene vacancies: The first-principles calculations," *Materials Today Communications*, vol. 19, pp. 459-463, 2019.

[28] A. Zelati, R. Taghavimendi, and A. Bakhshayeshi, "First-principles investigation of optoelectronic properties of novel SnS_2 with a cubic structure," *Solid State Communications*, vol. 333, p. 114344, 2021.

[29] R. Baghel, M. L. Verma, H. Kumar, and S. Verma, "Structural, electronic and optical properties of (P3HT)n in context of organic solar cells: DFT Based Approach," *2021 International Conference on Advances in Electrical, Computing, Communication and Sustainable Technologies (ICAECT)*, Bhilai, India, 2021, pp. 1-6.

[30] M. Amft, B. Sanyal, O. Eriksson, and N. V. Skorodumova, "Small gold clusters on graphene, their mobility and clustering: a DFT study," *Journal of Physics: Condensed Matter,* vol. 23, no. 20, p. 205301, 2011.

[31] Jogender, B. Badhani, Mandeep, and R. Kakkar, "A DFT-D2 study on the adsorption of phosgene derivatives and chloromethyl chloroformate on pristine and Fe_4-decorated graphene," *Journal of Molecular Graphics and Modelling,* vol. 101, p. 107754, 2020.

[32] G. Yu, Y. Xie, Q. Ge, Q. Dai, J. Xu, and H. Cao, "Mechanism of ozone adsorption and activation on B-, N-, P-, and Si-doped graphene: A DFT study," *Chemical Engineering Journal*, vol. 430, p. 133114, 2022.

[33] P. M. Singla, S. Riyaz, N. Singhal, and Goel, "Theoretical study of adsorption of amino acids on graphene and BN sheet in gas and aqueous phase with empirical DFT dispersion correction," *Physical Chemistry*, vol. 18, pp. 5597-5604, 2016.

[34] S. Zahid, A. Rasool, M. Ans, M. Yaseen, and J. Iqbal, "Quantum chemical approach of donor−π–acceptor based arylborane–arylamine macrocycles with outstanding photovoltaic properties toward high-performance organic solar cells," *Energy & Fuels*, vol. 35, no. 18, pp. 15018-15032, 2021.

[35] R. G. Parr, and R. G. Pearson, "Absolute hardness: companion parameter to absolute electronegativity," *Journal of the American Chemical Society*, vol. 105, no. 26, pp. 7512-7516, 1983.